

Star Formation Histories within the Antennae Galaxies (Arp 244)

Hong-Xin Zhang^{1,2,4}, Yu Gao^{1*} and Xu Kong³

¹*Purple Mountain Observatory, Chinese Academy of Sciences, 2 West Beijing Road, Nanjing, Jiangsu 210008, China*

²*Graduate School of the Chinese Academy of Sciences, Beijing 100080, China*

³*Center for Astrophysics, University of Science and Technology of China, Hefei 230026, China*

⁴*Current affiliation: Lowell Observatory, 1400 West Mars Hill Road, Flagstaff, AZ 86001, USA*

Accepted 2009 September 21. Received 2009 September 7; in original form 2009 May 14

ABSTRACT

With the imagery from *GALEX*, *HST*, *2MASS*, and *Spitzer*, and at the resolution of MIPS $24\ \mu\text{m}$ ($\sim 6''$), we study the variations of the broadband spectral energy distributions (SEDs) of star-forming regions within the nearest prototypal major merger — the Antennae galaxies. By including MIPS $24\ \mu\text{m}$ dust emission into stellar population analysis, we reliably, albeit roughly, constrain the star formation histories of these $24\ \mu\text{m}$ selected star-forming regions across the merging disks of the Antennae. Our population analysis is consistent with the star formation scenario that, most regions across the whole system are at a modest level of star formation with the exception of some localized intense starburst sites in the well-known *overlap* regions and the *western-loop* regions of northern galaxy NGC 4038. Compared with all the other regions, the young *overlap* regions currently (< 10 Myr) are experiencing much more violent enhancement of star formation. Across the *overlap* regions, we suggest two sequential star formation paths which we interpret as the imprints of the interpenetrating process of the two merging disks following their second close encounter. And we suggest that the star formation in the southern and (especially) northwestern edges of the *overlap* zone may have been just triggered by pre-starburst shocks. The well-known mid-infrared “hotspot” in the *overlap* regions is also a “hotspot” at $4.5\ \mu\text{m}$, whose total $4.5\ \mu\text{m}$ emission ($\geq 80\%$ from both hot dust and atomic/molecular lines) is comparable with that of the two galactic nuclei.

Key words: galaxies: individual (the “Antennae” galaxies) – galaxies: interactions – galaxies: stellar content – galaxies: starburst – galaxies: photometry

1 INTRODUCTION

Galaxy mergers, especially major mergers, can dramatically influence the morphological and star-forming properties of galaxies over relatively short timescales. Almost all the ultraluminous infrared galaxies (ULIRGs) — the strongest starbursts in the local Universe, are in interacting/merging systems (Sanders & Mirabel 1996). Moreover, Conselice, Chapman & Windhorst (2003) suggested that about two thirds of submillimeter galaxies at $z > 1$ are undergoing major mergers. Galaxy interactions/mergers seem to be very frequent in the past (e.g. Le Fevre et al. 2000; Peeters et al. 2002; Conselice et al. 2003; Elbaz & Cesarsky 2003; Kartaltepe et al. 2007; de Ravel et al. 2008; Lin et al. 2008; Conselice, Yang & Bluck 2009). Therefore, it is of

great importance to understand how the burst of star formation is triggered in the course of interacting/merging.

At a distance of 19.2 Mpc ($H_0 = 75\ \text{km s}^{-1}\ \text{Mpc}^{-1}$)¹, the Antennae (NGC 4038/39, Arp 244) is the nearest prototypal major merger between two gas-rich spiral galaxies (Toomre & Toomre 1972; Hibbard et al. 2001). Thus it provides us with a unique opportunity to study the induced star formation process as a consequence of interaction in detail. It has been extensively studied at essentially all wavelengths from X-ray to radio (Hummel & van der Hulst 1986;

¹ We note the recent debate about the distance to the Antennae. Saviane et al. (2008) determined a distance of ~ 13.3 Mpc from the tip of red giant branch, whereas Schweizer et al. (2008) estimated a distance of ~ 22.3 Mpc based on the type Ia supernovae 2007sr light curve. Throughout this work, we assumed the traditionally adopted Hubble Flow distance. However, our conclusions are not affected by the controversy over the distance.

* E-mail: yugao@pmo.ac.cn

Read, Ponman & Wolstencraft 1995; Vigroux et al. 1996; Mirabel et al. 1998; Nikola et al. 1998; Whitmore et al. 1999; Neff & Ulvestad 2000; Wilson et al. 2000; Fabbiano, Zezas & Murray 2001; Gao et al. 2001; Hibbard et al. 2001; Fabbiano et al. 2003; Fabbiano et al. 2004; Wang et al. 2004; Hibbard et al. 2005; Mengel et al. 2005; Bastian et al. 2006; Gilbert & Graham 2007; Schulz et al. 2007; Brandl et al. 2009). *ISO* mid-infrared (MIR) observations (Mirabel et al. 1998) show that the most intense starburst in this system takes place in the so-called *overlap* region between the two nuclei, which indicates its intermediate merging stage, almost totally obscured in the optical. Considering the abundant molecular gas, wide spread star formation and overall modest star formation efficiency, Gao et al. (2001) argued that Arp 244 has the potential of producing an ultraluminous extreme starburst in a later stage of merging.

In the Antennae, observations with *HST* have identified thousands of super star clusters (SSCs) (Whitmore et al. 1999) possibly being formed as part of the merging process. Both theoretical predictions (Goodwin & Bastian 2006) and observations (Whitmore 2004; Fall, Chandar & Whitmore 2005; Mengel et al. 2005) suggest that many of these SSCs will dissolve rapidly into the field stellar population in the course of galaxy-galaxy merging. This process was coined as star cluster's "*infant mortality*" (Whitmore 2004). Furthermore, a large number of stars may not form in star cluster mode. In fact, star clusters found in the deep *HST* images only contribute 9%, 8%, 5%, and 7% of the apparent total *U*, *B*, *V*, and *I* band light of the Antennae (Whitmore & Zhang 2002). Due to the uncertainties on the cluster formation history and efficiency, recently, Bastian et al. (2009) pointed out the difficulty in the accurate understanding of the age distribution of star clusters in mergers like the Antennae. Therefore, in order to obtain a complete picture of star formation histories in the course of merging, we must study the extended stellar populations, in addition to these star clusters.

Evolutionary population synthesis has become a powerful tool of interpretation of the integrated spectrophotometric observations of galaxies and sub-galactic regions. The most common method of model-observation comparison for stellar population analysis in galaxies is SED-fitting, with either least-squares or chi-squared minimization technique (e.g. Kong et al. 2000; Gavazzi et al. 2002). However, the well-known age-extinction degeneracy problem prevents us from obtaining reliable information about the star formation history for these galaxies or their sub-galactic regions, especially when only broadband photometry data are available. This is because these extended regions have an unknown mixture of various stellar populations, and the different populations may experience totally different extinctions (Calzetti, Kinney & Storchi-Bergmann 1994; Charlot & Fall 2000).

With the inclusion of the high-quality and high resolution *Spitzer* 24 μm dust emission data in our population analysis, we show here that the degeneracy between stellar population and dust extinction can be broken to a great extent. Thus, for the first time, we can reliably, albeit roughly, constrain the star formation histories within the Antennae galaxies using SEDs over the whole spectral range from far-UV (FUV) to MIR. The outline of this paper is the follow-

ing: In Sect. 2 we introduce the multi-band data that we use in this study, and give the multiwavelength photometry of star-forming regions selected mainly from the 24 μm image. Sect. 3 gives some brief comparisons of the broadband SEDs and their variations across the whole system. Sect. 4 presents our methodology to constrain the star formation histories across the merging disks, and the main results of our population analysis. We discuss these results in Sect. 5 and then a summary of our main findings follows in Sect. 6.

2 DATA AND PHOTOMETRY

2.1 Data

Both FUV ($\sim 1516 \text{ \AA}$) and near-UV (NUV; $\sim 2267 \text{ \AA}$) images were derived from the *GALEX* Ultraviolet Atlas of Nearby Galaxies distributed by Gil de Paz et al. (2007). The FWHMs of the PSFs are 5" and 6" at FUV and NUV, respectively. With these data Hibbard et al. (2005) have studied the stellar populations of the famous tidal regions.

Four broadband (F336W, F439W, F555W, F814W) and one narrowband (F658N; $\text{H}\alpha$) images (Whitmore et al. 1999) taken with the WFPC2 aboard the *HST* were obtained as B associations from the MAST Archive², and mosaic containing the four chips for each image was created.

NIR *JHKs* atlas images from *2MASS* were retrieved through the Interactive *2MASS* Image Service³.

The *Spitzer* imagery (3.6, 4.5, 5.8, 8.0, 24 μm) of the Antennae was obtained with both the Infrared Array Camera (IRAC; Fazio et al. 2004) and the Multiband Imaging Photometer for *Spitzer* (MIPS; Rieke et al. 2004) on board the *Spitzer Space Telescope*. The Basic Calibrated Data (BCDs) were retrieved with the Leopard software⁴. Background matching, cosmic-ray removal, flat-fielding and mosaicking were performed using the *Spitzer* Science Center's reduction software package MOPEX⁵. Images of the four IRAC bands have previously been presented by Wang et al. (2004).

2.2 Region Selection and Photometry Extraction

Prior to our multiwavelength photometry comparison and extraction, all images were background removed, registered/aligned, and resampled to the same pixel scale (1.5"). Then all images (except FUV/NUV) are convolved to the same resolution of MIPS 24 μm with the convolution kernels provided by Gordon et al. (2008).

We select star-forming regions primarily as 24 μm emission peaks, since 24 μm has been shown to be a very good local tracer of current star formation (e.g. Calzetti et al. 2005). Practically, we first use the *IRAF*⁶ DAOFIND task in DAOPHOT stellar photometry package (Stetson 1987)

² <http://archive.stsci.edu/hst/wfpc2/search.html>

³ <http://irsa.ipac.caltech.edu/applications/2MASS/IM/interactive.html>

⁴ Available at <http://ssc.spitzer.caltech.edu/propkit/spot/>

⁵ <http://ssc.spitzer.caltech.edu/postbcd/download-mopex.html>

⁶ *IRAF* is distributed by the National Optical Astronomy Observatories which are operated by the Association of Universities for Research in Astronomy, Inc., under cooperative agreement with the National Science Foundation

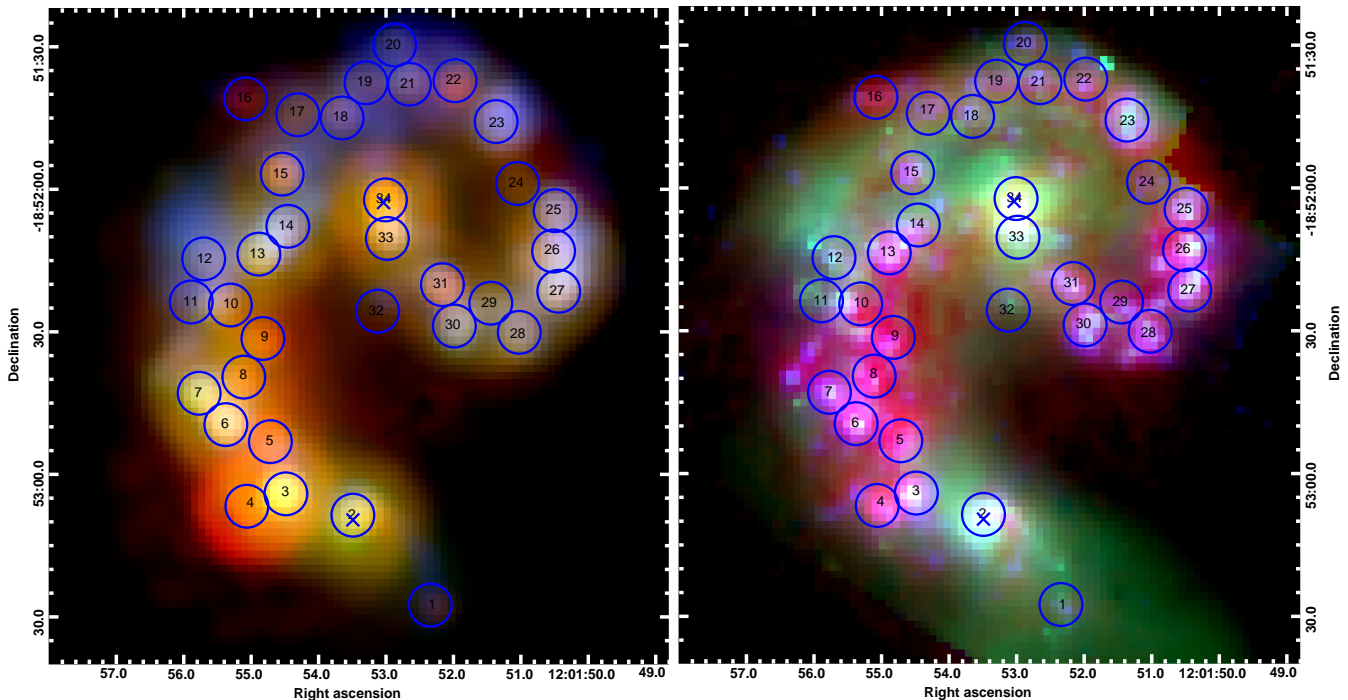


Figure 1. *Left:* Circular apertures of $9''$ in diameter were selected mainly as $24\mu\text{m}$ peaks and superposed on color-composite images generated from MIPS $24\mu\text{m}$ (red), *HST* $\text{H}\alpha$ (green), and *GALEX* FUV (blue) maps of the Antennae. The *HST* $\text{H}\alpha$ map has been degraded to match the resolution of MIPS $24\mu\text{m}$. The *cross* signs mark the nuclear centers of the two colliding galaxies. Pixel scales are $1.5''$. *Right:* Color composite image generated from the IRAC $8\mu\text{m}$ (red), *HST* F814W (green) and $\text{H}\alpha$ (blue) maps at their original resolutions (re-sampled to $1.5''$ pixel scales). The pixel scales of the two figures are $1.5''$. The original resolution of IRAC $8\mu\text{m}$ is $\sim 2''$. The mosaicked *HST* images originally have $\sim 0.1''$ pixels (undersampled). At the adopted distance, $1''$ corresponds to ~ 93 pc.

to find all local emission enhancements with 10σ signal-to-noise (S/N) ratio threshold in the $24\mu\text{m}$ image. Then we examine the findings of local enhancements visually and check carefully to ensure that these previously detected enhancements are true star-forming regions rather than artifacts due to the Airy diffraction rings or spikes. We also include three additional FUV bright regions without any nearby $24\mu\text{m}$ peaks associated (regions 11, 12 and 32). Finally, a total of 34 nearly non-overlapping circular apertures of $9''$ (~ 800 pc) in diameter (Figure 1) were selected. The large aperture size is mainly dictated by the PSF of $24\mu\text{m}$ and the rather extended emission features for most regions.

Our aperture size for photometry is, in any sense, significantly larger than a typical H II region (Knapen 1998; Oey et al. 2003), and even larger than a typical central star-forming region of a starburst galaxy. However, as is already found by Zhang et al. (2001), the spatial distribution of the young star clusters tends to be correlated up to physical scale of $\sim \text{Kpc}$. Bastian et al. (2006) have studied several star cluster complexes with sizes up to several hundred parsecs in the Antennae, they found that the young cluster complexes often share the same general velocity distribution with associated giant molecular clouds (GMCs), and even some complexes themselves are clustered. Our star-forming regions are usually spatially resolved into one or few such bright star cluster complexes dominated by few bright star clusters on the high-resolution optical/NIR imaging (e.g. Whitmore et al. 1999; Mengel et al. 2005). Therefore, most of our regions should be supposed to be complexes of star clusters over extended background stellar populations. We

note that some regions show slight, yet not systematic, displacement ($\sim 1 - 2''$) between the $24\mu\text{m}$ and the associated FUV peaks. The displacement may indicate that IR and UV emission are dominated by different clusters within these regions.

Although the measured FWHMs of the *GALEX* PSFs are close to that of the PSFs in MIPS $24\mu\text{m}$ image, we apply point source aperture corrections to FUV (1.206), NUV (1.269) and other bands (1.982). Aperture corrections are determined from photometry with increasing aperture radii of isolated field stars in the image fields. All the fluxes have been corrected for foreground Galactic extinction using a value of $E(B-V) = 0.046$ (Schlegel, Finkbeiner & Davis 1998) and Cardelli, Clayton & Mathis (1989) extinction law with $R_V = 3.1$. The uncertainties assigned to the photometric values are a quadratic sum of three contributions: variance of the local background, photometric calibration uncertainty (5% for FUV and WFPC2, 3% for NUV, 10% for IRAC, and 4% for $24\mu\text{m}$), and poisson statistics noise.

3 BROADBAND SEDS

Figure 2 shows the broadband SEDs for some representative regions across the Antennae galaxies as compared to that of entire Arp 220 and the local H II galaxy NGC 2798 (Kinney et al. 1993). There are some very remarkable differences of the SEDs between different regions across the whole system of the Antennae galaxies.

In the IR dust emission bands, $24\mu\text{m}$ very small

grains (VSGs) and $8\mu\text{m}$ PAH emission (for high-metallicity regions) all show very good correlation with extinction-corrected hydrogen recombination emission from starburst regions of normal galaxies to luminous IR galaxies (LIRGs) and ULIRGs (Alonso-Herrero et al. 2006; Calzetti et al. 2007). Nevertheless, the $8\mu\text{m}$ PAH emission is progressively depressed relative to $24\mu\text{m}$ with increasing star formation intensities (e.g. Calzetti et al. 2005; Smith et al. 2007; Draine & Li 2007; Thilker et al. 2007). Hence, the $24\mu\text{m}/8\mu\text{m}$ ratio would give a rough manifestation of different strengths of *current* star formation activities across the whole system.

Obviously, the *overlap* regions (3 - 9) generally have higher $24\mu\text{m}/8\mu\text{m}$ ratios than other regions in the Antennae, meaning that the *overlap* regions are the most intense *current* star-forming sites. *Spitzer* IRS spectrum (Brandl et al. 2009) also show that the *overlap* regions have overall the weakest relative strength (normalized to $15\mu\text{m}$ continuum flux) of PAH features among all these star-forming regions. High-resolution Optical and NIR observations (Whitmore et al. 1999; Mengel et al. 2005) suggest that the *overlap* regions host most of the youngest clusters. Region 4, which hosts the well-known MIR “hotspot” (Mirabel et al. 1998) of the *overlap* regions, has the highest $24\mu\text{m}/8\mu\text{m}$ ratios, even comparable with that of Arp 220. High-quality MIR spectrum (Brandl et al. 2009) obtained from *Spitzer* IRS more clearly show that region 4 is characterized by very hot dust emission and is among the regions with the strongest strength of the radiation field. The intrinsically brightest star cluster (WS95-80, Whitmore & Schweizer 1995) coincides with region 4.

The regions (16 - 22) in the *northern* galaxy NGC 4038 have the lowest $24\mu\text{m}/8\mu\text{m}$ ratios and reddest *UB* colors as compared with other regions, which is consistent with the fact that large number of rather old (100 Myr \sim 500 Myr) star clusters are found there (Whitmore et al. 1999; Mengel et al. 2005)

In the UV wavebands, on the contrary, the *Western-loop* regions (22-32) have the strongest UV emissions, largest UV excesses, and relatively strong $8\mu\text{m}$ (PAH) emissions, yet low $24\mu\text{m}/8\mu\text{m}$ ratios. These are in contrast with those in the *overlap* regions and indicate their relatively late star formation stage, which is also evidenced by the large $\text{H}\alpha$ bubbles found there (Whitmore et al. 1999). Brandl et al. (2009) also presents the IRS spectra of the UV brightest region 26, which has significantly weaker strength of the radiation field, yet stronger PAHs emission features, than do the *overlap* regions, in agreement with our broadband analysis.

The circumnuclear star-forming region of NGC 4038, namely region 33, has $24\mu\text{m}/8\mu\text{m}$ ratio close to that of the *overlap* regions, suggesting its intense *current* star formation activity. The prominent, yet redder, UV emission reveals that this region may also hold large post-starburst (> 10 Myr) stellar populations. For the two nuclei regions, NGC 4039 has both weaker $8\mu\text{m}$ PAH emission and $24\mu\text{m}$ dust emission indicating its lower star formation activity, whereas NGC 4038 has almost the same broadband SEDs as that of the local H II galaxy NGC 2798 in the plotted wavelength range. Thus far there is no strong evidence for the presence of AGN activity in the two nuclei. The IRS spectrum (Brandl et al. 2009) suggest that, both nuclei

regions have significantly weaker strength of the radiation field than the *overlap* regions. In comparison with the southern nucleus region, the northern nucleus region has flatter MIR continuum, stronger PAHs fluxes, yet smaller PAHs equivalent widths. These are consistent with our broadband analysis, i.e. both nuclei regions have weak *current* star formation strength compared to the *overlap* starburst regions, and the southern nucleus region has even weaker current star formation strength than does the northern nucleus. The stronger high excitation lines in the southern nucleus region (Brandl et al. 2009) should be attributed to supernovae shocks, which are also strongly evidenced by its very steep radio spectrum (Neff & Ulvestad 2000). We point out that our apertures covering the two nuclei (regions 2, 34) are so large that the surrounding star-forming regions are also included.

When we examine the SEDs variations across the *overlap* regions, we see an interesting phenomenon. From the central regions, i.e. regions 6 and 7, to both the northwestern (e.g. regions 8, 9) and southeastern (e.g. regions 4) regions, the UV/optical emission gradually become redder and weaker, accompanying with comparable amount of energy fraction re-emitted as IR dust emission. In the following sections, we show that the obvious trends of the SEDs variations across the *overlap* regions may reflect the star formation modes in the *overlap* regions.

4 STELLAR POPULATION ANALYSIS

4.1 Methodology

The availability of $\text{H}\alpha$ and MIPS $24\mu\text{m}$, which traces the star formation (unobscured and obscured) on timescales of ~ 10 Myr, FUV and NUV (tracing star formation on timescales of ~ 100 Myr), and the $U(\text{F336W})$ and $B(\text{F439W})$, whose combination in U/B ratio is sensitive (straddles the 4000\AA break) to the fraction of populations younger than a few hundred Myr relative to the old populations, makes it reasonable to roughly probe the star formation histories across the whole merging disks of the Antennae. With χ^2 minimization technique, we fit the broadband SEDs (FUV- K_s) plus the narrowband $\text{H}\alpha$ photometry for the above selected star-forming regions with superpositions of three single stellar populations (SSPs), namely young (< 10 Myr), intermediate (10 Myr-300 Myr) and old (> 300 Myr) populations. In our fitting, we account for the different extinctions experienced by different populations.

For population synthesis models, we use the new version Starburst99 (Vazquez & Leitherer 2005) SSP models with the Padova 2000 stellar evolution tracks, which include the full AGB evolution. We adopt the multi-power law Kroupa initial mass function (Kroupa 2002). Adoption of the bottom-heavy Salpeter IMF would not change our main conclusions in this paper. Using the metallicity sensitive Mg I line at 8806.8\AA , Mengel et al. (2002) found a handful of star clusters in Arp 244 with solar metallicity, which is consistent with recent metallicity estimation (Bastian et al. 2009) from more absorption and emission lines in the Antennae. Thus, we fix solar metallicity for all the SSPs models. Since we have narrow-band $\text{H}\alpha$ imagery data, and the regions we studied are all actively star-forming regions, we include gaseous emission into the SSP

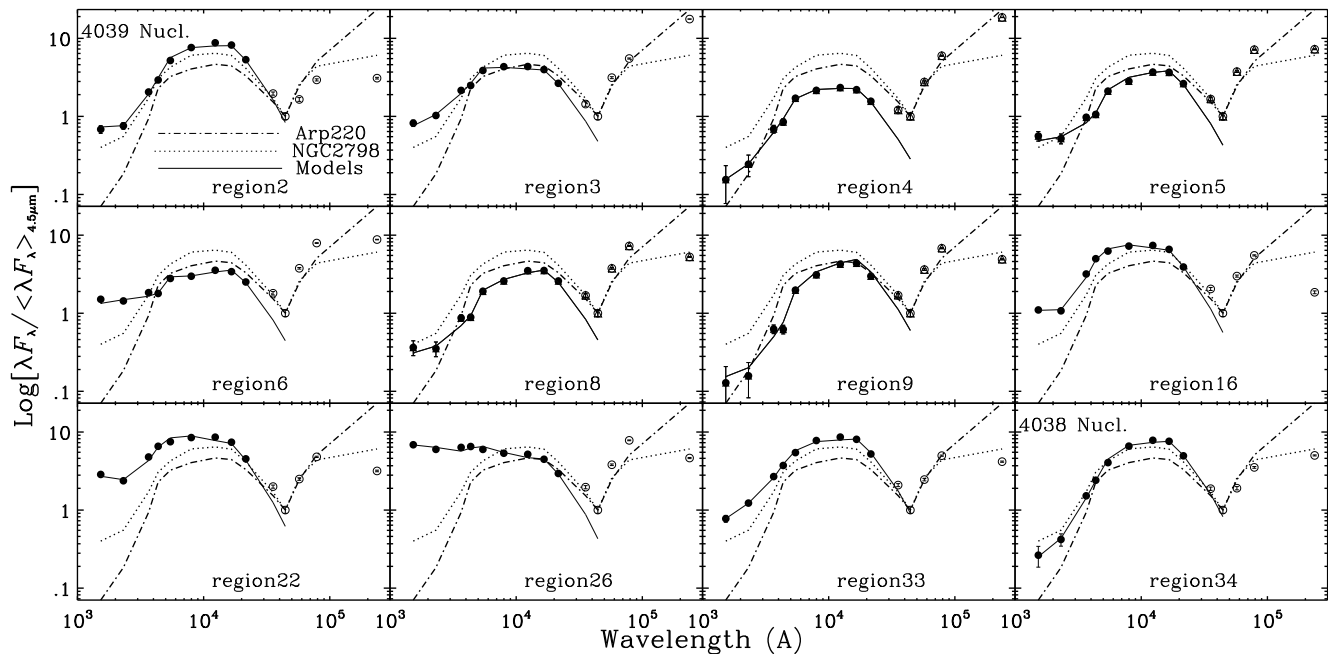


Figure 2. Display of FUV-24 μm broadband SEDs of some representative star-forming regions marked in Figure 1 and compared to Arp 220 and local H II galaxy NGC 2798. The broadband photometry data points from FUV to K_s , which are fitted with 3-SSP superpositions, are represented by *filled circles* and the *Spitzer* data points by *open circles*. For the purpose of comparison, the broadband WFC2 data have been transformed to standard *UBVI* system with the transformation coefficients provided by Holtzman et al. (1995). The best-fit (FUV- K_s) composite stellar broadband SED models have been plotted as *solid lines*.

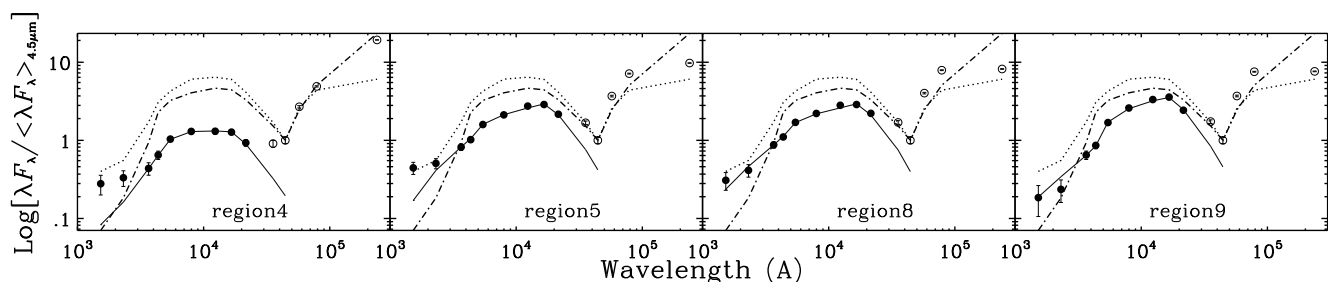


Figure 3. Display of FUV-24 μm broadband SEDs (extracted from the images with their *original resolutions*) of four *overlap* star-forming regions, which may have significant starlight contamination by nearby bright regions at short wavebands. Lines and symbols are the same as in Figure 2, except that FUV/NUV data are not used in the SED-fittings. It can be seen that the overall shapes of the SEDs do not change as compared with the SEDs extracted from the smoothed images (Figure 2).

models. Besides the nebular continuum emission and several hydrogen emission lines provided by Starburst99, we also account for other strong hydrogen emission lines (i.e. Balmer, Paschen, Brackett and Pfund lines) assuming case B recombination and strong non-hydrogen element emission lines using the line ratios of typical Galactic H II regions compiled by Anders & Fritze-v. Alvensleben (2003).

For dust extinction, we use the two-phase dust attenuation recipes developed by Charlot & Fall (2000). The effective absorption curve is proportional to $\lambda^{-0.7}$. One adjustable parameter μ defines the ratio of the total effective extinction experienced by intermediate/old (> 10 Myr) to young (< 10 Myr) populations.

It is becoming well known, from the works of the SINGS team, that the combination of $H\alpha$ and 24 μm accounts for both the unobscured and obscured current star formation for star-forming regions in galaxies (Calzetti et al. 2007;

Kennicutt et al. 2007). We adopt the relationship between extinction-corrected $H\alpha$, observed $H\alpha$ and 24 μm calibrated for the H II regions in the 33 SINGS galaxies (equation 5 in Calzetti et al. (2007)) to obtain the $H\alpha$ extinction, and then use the Charlot & Fall (2000) extinction curve to derive the approximate A_V of the young stellar populations from the following equation

$$A_V = 2.825 \log \left[1 + 0.031 \frac{L_{24\mu\text{m}}}{L_{H\alpha}} \right] \quad (1)$$

where $L_{24\mu\text{m}}$ is the dust-only 24 μm monochromatic luminosity and $L_{H\alpha}$ is the observed $H\alpha$ luminosity.

Therefore, we first restrict the variations of the three SSPs to their corresponding age ranges mentioned above in order to model the SEDs of various star-forming regions across the merging disks in the Antennae galaxies. Then

we try to find the best-fit composite models with the χ^2 minimization technique

$$\chi^2 = \sum_{i=\text{FUV}}^{K_s} \left(\frac{F_{\text{obs},i} - aF_{\text{mod},i}}{\sigma(F_{\text{obs},i})} \right)^2 \quad (2)$$

by minimizing Equation 2. In this way, we obtain the four best-fit parameters, namely, the mass of the old (M_o), intermediate (M_i) and young (M_y) populations, the extinction ratio (μ) of intermediate/old to young populations. It should be stressed here that we first fix the extinction A_V with Equation 1 prior to SED modeling, which affects mostly the young stellar populations. This makes our stellar population analysis presented in this paper much less affected by the degeneracy between stellar population and extinction.

4.2 Results of SED-fitting

4.2.1 Best-fit Parameters

Our main fitting results are summarized in Table 1. One should keep in mind that, we are actually comparing relatively clustered younger stellar populations with relatively extended older populations. Hence, the absolute values for the mass ratios between different populations should be sensitive to the size of photometric apertures and the average density of the underlying stellar populations. On that account we mainly focus on the relative changes of the mass ratios between different populations across the system.

We notice that the SED-fitting quality for some *overlap* regions (i.e. regions 8, 9), is not as good as for most other regions (Figure 2). The possible reason can be either the significant starlight contamination by nearby bright regions or the very faint nature (low S/N ratio) of these two regions at short wavebands. To check the significance of the starlight contamination by nearby bright regions, we also present the broadband SEDs for the four optically faint regions in the *overlap* region in Figure 3. It can be seen that the contamination by nearby bright regions does not change the overall SEDs shape for these regions. In fact, when we fit the SEDs (excluding the FUV/NUV data) extracted from the images at their original resolutions for these regions, our main conclusions for the *overlap* regions do not change. Table 2 lists the fitting results for the *overlap* regions using SEDs extracted from the images at their original resolutions. According to our best-fitting results for these regions, the best-fit ages of intermediate populations $\lesssim 100$ Myr, and the best-fitting ages of old stellar population ≥ 3 Gyr.

For the mass ratios of intermediate to old populations M_i/M_o , the *overlap* regions have overall smaller values compared to other regions, suggesting the *overlap* star-forming regions are very young. Northern edge of the *overlap* regions, i.e. region 9, for example, has the lowest M_i/M_o . Whereas the *western-loop* regions of NGC 4038 have overall the largest M_i/M_o across the whole system, and they are the brightest regions in UV. The *western-loop* regions host most of the intermediate populations. The ratios of most other regions across the whole system fall in between the *overlap* and *western-loop* regions.

For the mass ratios of young to old populations M_y/M_o , the *overlap* regions and some *western-loop* regions have M_y/M_o larger than all the other regions. The similar con-

trast could also be seen from the age-averaged mass fraction ratios of young to old populations ($\frac{M_y/\text{Age}_y}{M_o/\text{Age}_o}$). The *overlap* and *western-loop* regions host most of the young populations, and they are the most intense current star-forming sites across the whole system.

For the mass ratios of young to intermediate populations M_y/M_i , the *overlap* regions hold the largest values, while the *northern* regions have overall small M_y/M_i , conforming with their weak *current* star formation activities. We also point out here one interesting finding. That is, across the *overlap* regions, the northwestern edge, namely region 9, and the southeastern edge, region 4, have the M_y/M_i ratios significantly larger than the central regions, e.g. region 6. We note that the trend still exist after we normalize the mass fraction ratios with their corresponding best-fit ages ($\frac{M_y/\text{Age}_y}{M_i/\text{Age}_i}$).

In the last column of Table 1, we also list the corresponding total starlight absorbed by dust which should be equal to the total infrared (TIR) dust emission. Calzetti et al. (2005) exploited a relationship between $24\mu\text{m}/\text{TIR}$ and $8/24\mu\text{m}$ for the star-forming regions in NGC 5194. Considering the similar global properties between the Antennae and NGC 5194, such as similar PAH abundances (the PAH index ~ 4.5 according to Draine & Li (2007) dust emission models), comparable TIR (Sanders et al. 2003) and total molecular gas surface density (Wilson et al. 2003), we compare the total starlight absorption from our models with the TIR estimated from dust-only $8\mu\text{m}$ and $24\mu\text{m}$ using the relation (equation 1 in Calzetti et al. 2005) exploited for the star-forming regions of NGC 5194. The comparison is shown in Figure 4. Obviously, almost all our selected star-forming regions in Arp 244 generally follow the same relation derived in the star-forming regions of NGC 5194. Considering the general consistency, in the following sections, we take the total starlight absorption from our SED-fitting models as the best estimate of TIR for our selected star-forming regions.

4.2.2 Star-Forming Regions of Arp 244 on the IRX-UV Plane

Kong et al. (2004) found that, while the dust extinction is the main factor driving the strong correlation between $L_{\text{TIR}}/L_{\text{FUV}}$ (hereafter IRX) and UV spectral slope, it is the star formation history that affects the degree of deviation of a star-forming galaxy from the locus of starbursts in the IRX-UV color indices' plane. It is surely meaningful to plot these indices for the star-forming regions of the Antennae on the IRX-UV color plane. Figure 5 shows the ratio of $L_{\text{TIR}}/L_{\text{FUV}}$, where TIR is set to be equal to the total starlight absorption obtained from our models, as a function of β_{GLX} ($\beta_{\text{GLX}} = \frac{\log F_{\text{FUV}} - \log F_{\text{NUV}}}{\log \lambda_{\text{FUV}} - \log \lambda_{\text{NUV}}}$; see Kong et al. 2004). The solid line represents the tight correlation for starburst galaxies (Kong et al. 2004). Obviously, except the *overlap* regions, almost all the star-forming regions in Arp 244 lie below the locus followed by starbursts. The three regions that lie above the starburst locus are region 4, 5 and 9. Hence, it can be stated here that except for some localized starburst sites, mainly in the *overlap* regions, most regions across the whole system are forming stars at a level weaker

Table 1. SED-fitting Results.

Reg.	χ_r^2	μ	M_i/M_o	M_y/M_o	M_y/M_i	$\frac{M_y/Ag_{ey}}{M_i/Ag_{ei}}$	$\frac{M_y/Ag_{ey}}{M_o/Ag_{eo}}$	$\log[\text{Total Abs.}]$ (erg/s)
NGC4039 Arms								
1	1.1	0.1	0.003	7.0e-4	0.23	2.6	0.5	41.71
Southern Nucleus								
2	2.2	0.9	0.03	6.0e-4	0.02	3.8	1.7	42.72
Overlap Regions								
3	2.5	0.6	0.03	0.003	0.1	6.3	20.2	43.09
4	2.7	0.3	0.01	0.007	0.7	10.4	11.3	43.21
5	4.3	0.4	0.002	0.001	0.5	7.5	12.6	42.67
6	2.3	0.8	0.008	0.002	0.2	3.7	29.0	42.82
7	4.5	1.0	0.007	0.002	0.3	8.0	9.6	42.53
8	4.2	1.0	0.004	7.0e-4	0.2	11.1	6.1	42.61
9	5.9	0.8	<1.0e-4	4.0e-4	>4.0	>40.0	3.0	42.46
Eastern Regions								
10	3.0	0.9	0.01	5.0e-4	0.03	1.5	5.3	42.55
11	1.8	1.0	0.05	5.0e-4	0.01	0.2	2.1	42.46
12	1.9	0.9	0.05	4.0e-4	0.008	0.4	5.0	42.55
13	2.8	1.0	0.01	7.0e-4	0.07	1.3	3.4	42.60
14	2.1	0.3	0.01	6.0e-4	0.06	2.0	8.7	42.28
15	0.9	0.5	0.04	5.0e-4	0.01	1.3	4.3	42.36
Northern Regions								
16	1.3	0.1	0.07	6.0e-4	0.008	1.5	1.7	41.57
17	1.5	0.2	0.1	6.0e-4	0.005	1.1	1.7	41.82
18	1.1	0.2	0.04	3.0e-4	0.007	0.7	4.3	41.91
19	1.0	0.3	0.05	3.0e-4	0.006	0.6	3.7	41.89
20	1.1	0.2	0.07	4.0e-4	0.006	0.6	3.4	41.62
21	1.2	0.1	0.04	4.0e-4	0.009	0.9	5.8	41.78
22	2.2	0.1	0.06	0.001	0.02	1.7	2.8	41.92
Western-Loop Regions								
23	0.5	0.5	0.03	6.0e-4	0.02	0.3	4.4	42.42
24	2.3	0.7	0.09	4.0e-4	0.004	0.7	2.9	42.09
25	3.1	0.8	0.03	8.0e-4	0.02	0.8	11.6	42.46
26	1.9	0.7	0.2	0.007	0.04	0.5	50.0	42.72
27	3.1	1.0	0.2	0.006	0.03	0.4	29.6	42.72
28	3.8	1.0	0.2	0.002	0.01	1.3	17.4	42.30
29	3.1	1.0	0.2	0.003	0.02	1.8	3.0	42.26
30	3.0	1.0	0.1	0.002	0.02	0.6	3.2	42.43
31	2.5	0.7	0.03	7.0e-4	0.02	1.2	7.4	42.50
32	2.6	0.1	0.02	0.002	0.1	8.0	1.5	42.05
Circumnuclear Regions of NGC4038								
33	1.1	0.8	0.03	4.0e-4	0.01	0.3	1.3	42.90
Northern Nucleus								
34	1.4	0.6	0.01	7.0e-4	0.05	1.5	1.4	43.03

χ_r^2 is the reduced minimum χ^2 value. μ is the extinction ratio of intermediate/old to young populations. M_y , M_i and M_o represent the mass of young, intermediate and old populations respectively. $\frac{M_y/Ag_{ey}}{M_i/Ag_{ei}}$ and $\frac{M_y/Ag_{ey}}{M_o/Ag_{eo}}$ represent the corresponding age-averaged mass fraction ratios. The total starlight absorption obtained from the models is listed in the last column.

Table 2. Fitting Results for the SEDs (without FUV/NUV) extracted from the images at their original resolutions. Only results for some of the *overlap* regions which may have significant mutual light contamination are listed.

Overlap Regions								
Reg.	χ_r^2	μ	M_i/M_o	M_y/M_o	M_y/M_i	$\frac{M_y/Ag_{ey}}{M_i/Ag_{ei}}$	$\frac{M_y/Ag_{ey}}{M_o/Ag_{eo}}$	$\log[\text{Total Abs.}]$ (erg/s)
3	1.0	0.5	0.04	0.01	0.3	5.0	40.0	42.97
4	0.3	0.3	0.01	0.05	4.5	9.4	100.1	43.50
5	0.7	0.8	0.004	0.005	1.3	4.7	13.5	43.11
6	1.9	1.0	0.05	0.01	0.2	1.5	73.0	42.94
7	1.8	0.3	0.02	0.004	0.2	2.9	42.5	42.54
8	0.9	1.0	0.04	0.002	0.05	0.6	8.8	42.82
9	1.0	0.7	0.002	0.001	0.5	5.0	4.2	42.52

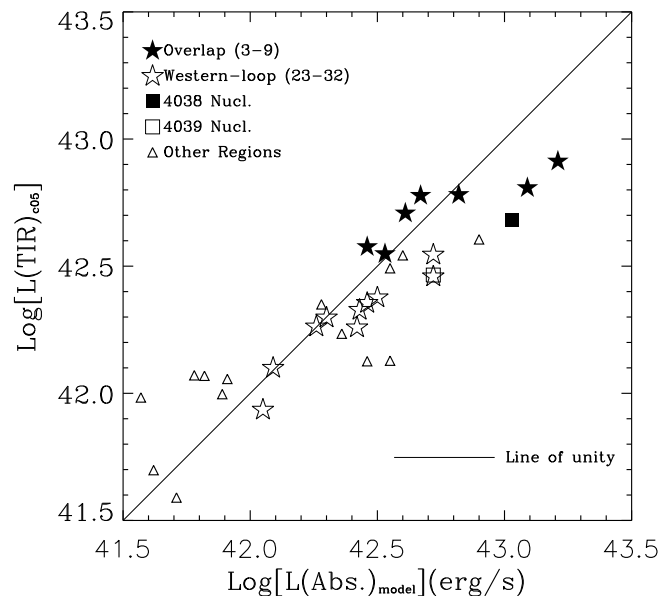


Figure 4. Total starlight absorption obtained from the SED-fitting models is compared with total infrared luminosity estimated from dust-only $24\ \mu\text{m}$ and $8\ \mu\text{m}$ using the relation calibrated in NGC 5194 by Calzetti et al. (2005) (hereafter TIR_{c05}). The line with slope of unity and null intercept is also plotted (solid line).

than that of the starbursts. This is also consistent with our further analysis on star formation histories.

Figure 6 plots the ratios of $L(H\alpha_{\text{corr}})/L(Ks)$ vs. $L_\lambda(U)/L_\lambda(B)$. Star-forming regions in NGC 5194 selected (mainly as $24\ \mu\text{m}$ peaks) by Calzetti et al. (2005) are shown as small *pluses*. Also plotted is the archetypical starburst galaxy NGC 7714 as a whole (*large cross*). The modest total star formation rate ($\sim 3.4\ M_\odot\text{yr}^{-1}$) and star formation intensity ($\sim 0.015\ M_\odot\text{yr}^{-1}\text{Kpc}^{-2}$) of NGC 5194 place it among the quiescently star-forming galaxies, although it hosts a LINER-type nucleus. Calzetti et al. (2005) found that the star-forming regions in NGC 5194 have properties quite similar to that of the normal star-forming galaxies, rather than that of starbursts. Assuming $L_\lambda(U)/L_\lambda(B)$ and $L(H\alpha_{\text{corr}})/L(Ks)$ roughly represent the ratios of recent-to-past and current-to-past star formation strengths, respectively, Figure 6 reveals similar results as that of the IRX-UV diagram. Namely, almost all the star forming regions of Arp 244 have current star formation strength comparable with star-forming regions in quiescently star-forming galaxies (low $L(H\alpha_{\text{corr}})/L(Ks)$), except for some of the *overlap* and *western-loop* regions.

4.2.3 Emission Excess at IRAC $3.6\ \mu\text{m}$ and $4.5\ \mu\text{m}$

Since we have done relatively sophisticated SED-fitting for these star-forming regions, we could estimate the hot dust emission at IRAC $3.6\ \mu\text{m}$ and $4.5\ \mu\text{m}$ which are often assumed to be dominated by stellar photospheric emission in literatures. With the average of $3.6\ \mu\text{m}$ and $4.5\ \mu\text{m}$ fluxes as the underlying stellar continuum level, Wang et al. (2004) concluded that most of the emission ($>90\%$) in these two bands comes from direct stellar contribution for the whole system. From our stellar SED-fitting, we could easily see

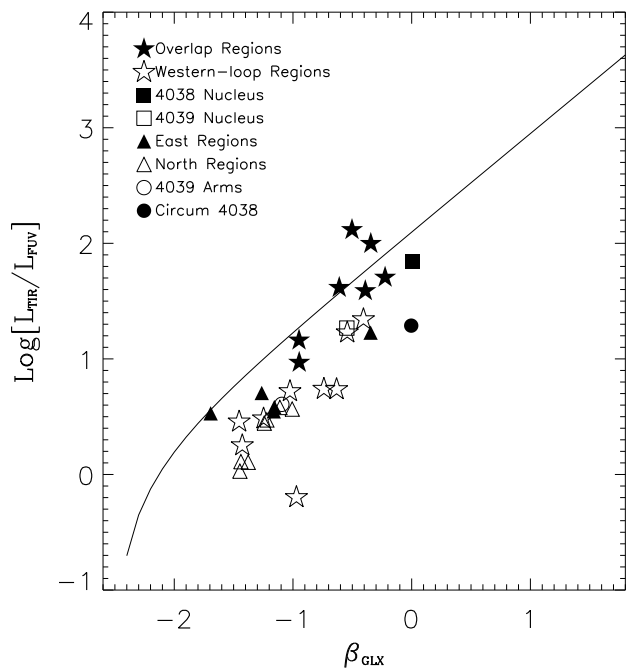


Figure 5. Ratio of TIR (set to total starlight absorption from models) to FUV luminosity as a function of equivalent ultraviolet spectral slope (the IRX-UV diagram). Data for different star-forming regions within the Antennae are plotted with different symbols. The solid line represents the mean IRX-UV relation for 50 starburst galaxies fitted by Kong et al. (2004).

(Figures 2 and 3) the prominent emission excess at $3.6\ \mu\text{m}$ ($\sim 10\% - 65\%$) and $4.5\ \mu\text{m}$ ($\sim 10\% - 80\%$) for most of these star-forming regions relative to the stellar (plus nebular continuum) emission, especially for the *overlap* regions. The significant emission excess at $3.6\ \mu\text{m}$ and $4.5\ \mu\text{m}$ brings out the caution needed in using them as representation for the underlying stellar mass, particularly when studying the active star-forming regions. Since we have largely accounted for hydrogen/helium recombination emission in our SED-fitting, according to the existing observations of spectra in these two bands of compact H II regions (e.g. Martin-Hernandez et al. 2000; Peeters et al. 2002), the other possible main mechanisms of the emission excess could be vibrationally excited molecular hydrogen emission, atomic fine-structure lines, or very small hot dust (e.g. $3.3\ \mu\text{m}$ PAH feature) emission.

For region 4, the MIR “hotspot”, the excess emission components contribute $\geq 65\%$ and 80% ⁷ of the total emission at $3.6\ \mu\text{m}$ and $4.5\ \mu\text{m}$ respectively. As is already pointed out by Wang et al. (2004), the extremely high obscuration of region 4 must be responsible for the large excess to some extent. The high-quality MIR spectrum of this region obtained from IRS on board *Spitzer* is characterized by prominent PAHs and very hot VSGs emission (Brandl et al. 2009). Given the prominent PAH feature emission of region 4, the exceptionally low excess emission flux ratio of $3.6\ \mu\text{m}/4.5\ \mu\text{m}$ (~ 0.9) can not be accounted for by the pure dust emission models of Draine & Li (2007). Furthermore, the *K*-band spectra (Gilbert et al. 2000) in the obser-

⁷ Considering the hot dust emission contribution to *Ks* band, our estimation should be lower limits.

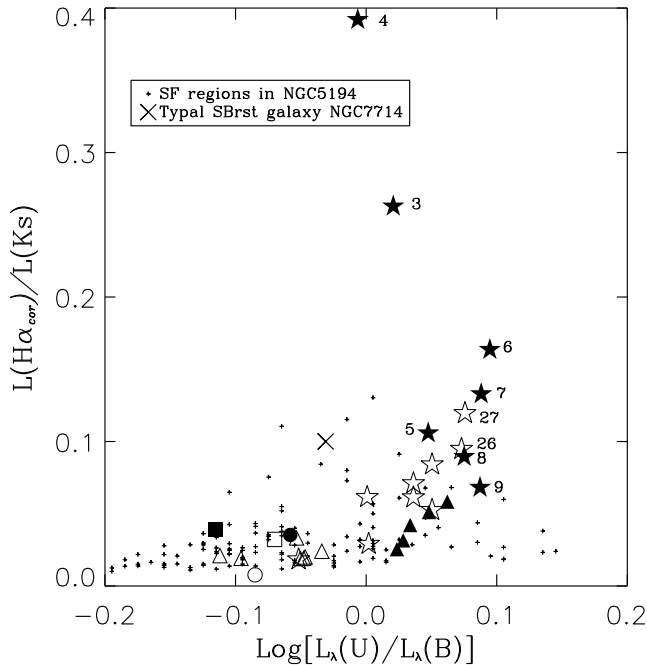


Figure 6. Ratio of extinction-corrected (using $24\ \mu\text{m}$) $L(H\alpha_{corr})$ to $L(Ks)$ vs. $\log[L_\lambda(U)/L_\lambda(B)]$. The symbols are as Figure 5. The star-forming regions selected by Calzetti et al. (2005) in the quiescently star-forming galaxy NGC 5194 are shown by small pluses. The archetypal starburst galaxy NGC 7714 as a whole is represented by large cross. Obviously, just like the majority of star-forming regions in NGC 5194, most regions (except some of the *overlap* and *western-loop* regions) in Arp 244 host a significant fraction of older stellar populations and have relatively lower current star formation strength compared to typical starbursts. See the text for further explanation.

vations of the compact star clusters coincident with the MIR “hotspot” are characterized by prominent nebular and fluorescent H_2 emission with slightly rising continuum toward the red (due to hot dust emission). The fact that region 4 has very flat radio spectrum (Neff & Ulvestad 2000) and prominent PAH feature emission excludes the shock origin of the possible molecular/atomic emission. Thus, the fine-structure lines from heavy elements, the molecular lines from FUV fluorescence in dense photodissociation regions (PDRs) and hot dust (including PAHs) emission may all have significant contribution to the emission excess at IRAC $3.6\ \mu\text{m}$ and $4.5\ \mu\text{m}$.

Interestingly, the total $4.5\ \mu\text{m}$ flux of region 4 is even $\sim 20\%$ higher than that of the southern nucleus and nearly equal to that of northern nucleus. In short, the excess emission (either from hot dust or molecule/ionized atoms) at IRAC $4.5\ \mu\text{m}$ bands have nonnegligible ($> 18\%$ ⁸) contribution to the total flux for the whole system.

⁸ This is obtained by the sum of flux of excess emission for all the star-forming regions selected in this work divided by the total flux for the whole system. So here our estimation is a lower limit for the whole system.

5 DISCUSSION

5.1 Star Formation Histories Across the Whole System

Since we have the mass ratios between the three stellar populations for these star-forming regions, using the best-fit ages of the three populations for each region, we could easily derive the ratios between the age-averaged star formation rate (SFR) for the three (i.e. current, recent and past) star formation epochs related to our three populations (Table 1 and 2). We find that, except for some of the *overlap* regions and the *western-loop* regions of NGC 4038, which have the ratios of *current-to-past* age-averaged SFR (defined approximately as $\frac{M_V/Ag_{ev}}{M_I/Ag_{ei}} \gtrsim 10$, almost all the other star-forming regions have the ratios $\gtrsim 1$. Specifically, the regions which have the ratios $\gtrsim 10$ are 3, 4, 5, 6, 25, 26, 27, and 28. Hence, it can be said that, some of the *overlap* and *western-loop* regions are experiencing bursts of star formation, whereas most of the other regions are forming stars at a moderate level comparable with normal star-forming galaxies. The location of these star-forming regions on the IRX-UV plane (Figure 5) is also consistent with the fact that most of the regions are at a modest star formation intensity. For the ratios of *current-to-recent* age-averaged SFR (defined as $\frac{M_V/Ag_{ev}}{M_I/Ag_{ei}}$) (see Table 1), the *overlap* regions have the ratios $\gtrsim 3$, whereas almost all the other regions have the ratios ~ 1 . The high $\frac{M_V/Ag_{ev}}{M_I/Ag_{ei}}$ for the two nuclei may be attributed to their surrounding star-forming regions. Hence, comparing with the *overlap* regions, the star formation of most regions across the whole system is not only modest (except the *western-loop* regions) but also continuous during the recent tens of million years (typical best-fit ages of the intermediate stellar populations for these regions). Namely, while both the *overlap* regions, and the *western-loop* regions are the most intense *current* star-forming sites across the whole system, the *overlap* regions are now experiencing much more violent enhancement of star formation compared to all the other regions.

In fact, the star formation histories for these star-forming regions could also be simply probed through the ratios of $L_\lambda(U)/L_\lambda(B)$ and $L(H\alpha_{corr})/L(Ks)$, which roughly represent ratios of the recent-to-past star formation strength and the current-to-past star formation strength, respectively. Figure 6 clearly shows that, except for the *overlap* and *western-loop* regions, most regions are forming stars at moderate level (low $L(H\alpha_{corr})/L(Ks)$) comparable with star-forming regions in quiescently star-forming galaxies. And meanwhile these regions host a remarkable fraction of aging stellar populations (small $L_\lambda(U)/L_\lambda(B)$), just like the star-forming regions in NGC 5194. The overall larger ratios $L_\lambda(U)/L_\lambda(B)$ for the *overlap*, the *western-loop* and the *eastern* (to a lesser extent) regions compared with the star-forming regions in quiescently star-forming galaxies indicate that these regions may have just experienced a period of intense starburst in the recent few hundred million years. It is also notable of the much higher ratios of current-to-past star formation strength for some of the *overlap* and *western-loop* regions. Wang et al. (2004) also got similar results from the flux ratio of the dust-only IRAC $8\ \mu\text{m}$ and the underlying stellar continuum.

5.2 *The 20 cm-to-CO ratio map as star formation efficiency map*

Taking advantage of the tight correlation between FIR and radio continuum (Condon 1992; Yun et al. 2001; Bell 2003), which appears to be valid at least on kiloparsec scales in galaxies (Lu et al. 1996), Gao et al. (2001) constructed a star formation efficiency map using the 20 cm-to-CO ratio. Overall, our results of population analysis are consistent with their star formation efficiency map, viz, except some localized starburst sites mainly in the *overlap* and *western-loop* regions, most regions across the whole system are forming stars at a quite moderate level comparable with normal star-forming galaxies. This verifies the practice of using radio continuum as an indicator of the star formation and the radio-to-CO ratio maps as representation of star formation efficiency maps in most cases.

Nevertheless, some exceptions do exist, like for some *overlap* regions of galaxy pairs in high-speed collision. For instance, in the Taffy galaxy a large portion of the synchrotron radio emission may be related to gas collision shocks, rather than supernovae remnants (SNRs, most likely related to recent star formation) shocks (Gao et al. 2003; Zhu et al. 2007). In the *overlap* regions of the Antennae, Gao et al. (2001) found that the radio-to-CO ratios progressively increase from the southeastern side to the northwestern edge across the *overlap* regions. However, we note that, the lower radio-to-CO ratio of the southeastern region (4) compared to other *overlap* regions may be, rather than due to lower star formation efficiency, assigned to other various causes. First, the very flat radio continuum suggests that the 20 cm continuum in region 4, rather than being dominated by synchrotron emission from (maybe) SNRs shocks like other *overlap* regions, is primarily thermal free-free emission from young, compact H II regions. This means that, in such violent *overlap* starburst environment, large numbers of supernovae events associated with current star formation epoch have not happened. Second, studies on the local IR/radio correlation within nearby galaxies (e.g. Hughes et al. 2006; Murphy et al. 2006) demonstrate the weak trend of increasing IR/radio ratio with increasing IR luminosity within individual galaxy. Both our TIR estimates (equal to the total starlight absorption) and recent IR estimate based on the 15 μm and 30 μm continuum fluxes (Brandl et al. 2009) suggest that region 4 has the largest IR luminosity across the whole system. Finally, the very hot dust emission, as we have shown above, for the southeastern side (i.e. region 4) implies that most energy there may emit in the MIR regime, which again is different from most of the other regions. Therefore, unlike the usually continuous star formation in a relatively long timespan ($\geq 10^8$ yr), in the violent galaxies interaction regions, both the strong shocks as a result of cloud-cloud collisions and the strong variations of star formation rate in short timescales (tens of Myr) may all make the 20cm-to-CO ratio fails to be an efficient star formation efficiency indicator.

5.3 *Sequential Star Formation Paths in the Overlap Regions*

Across the *overlap* regions (Table 1 and 2), the northwestern edge and the southeastern edge have both higher mass ratios

of young to intermediate populations M_y/M_i (i.e. regions 9 and 4) and higher correspondingly age-averaged SFR ratios $\frac{M_y/Ag_{ev}}{M_i/Ag_{ei}}$ than do the central regions (e.g. regions 6). We like to interpret the trends as two sequential star formation paths. One is from the central regions (i.e. regions 6) to the *southern* edge (e.g. region 4), and the other is from the central to the *northwestern* edge (e.g. region 9).

To check if there are any trends for the spatial distributions of the star clusters across the *overlap* regions, we refer to the cluster distribution maps derived by Zhang et al. (2001). We find a slightly proportionally deficit of clusters with ages of tens of Myr for both the northwestern (corresponding to our region 9) and the southern edges compared to the central regions (e.g. region 6). Recently, Mengel et al. (2005) also obtained the spatial distributions for clusters with Br γ -determined and CO-index-determined ages. Interestingly, the distributions also show the relative deficit of intermediate-age (~ 10 Myr) clusters for both the northwestern and southern edges, although the sample size and the probed age range are all small compared to that of Zhang et al. (2001). The cluster distributions are in agreement with the sequential star formation paths mentioned above, i.e. both the *northwestern* and *southern* regions are just beginning their recent star formation episode.

Jog & Solomon (1992) proposed a physical mechanism to explain the origin of the enhanced star formation occurring in situ in the overlapping regions of a pair of colliding galaxies like the Antennae. In their model, following a collision between galaxies, the H I cloud-cloud collisions from the two galaxies lead to the formation of hot, ionized, high-pressure remnant gas that compresses the outer layers of pre-existing GMCs in the overlapping regions. This makes the GMCs shells become gravitationally unstable, which triggers a starburst in the initially barely stable GMCs. Although generally H I cloud-cloud collisions should be more efficient than that of the GMCs due to the much smaller mean free path of an H I cloud than GMC, the huge concentration of molecular gas in the *overlap* regions of Arp 244 (Wilson et al. 2000; Gao et al. 2001) may make the GMCs collisions also possible.

Based upon this model, across the *overlap* regions of Arp 244, the sequential star formation paths we have found can be explained naturally. As the two colliding disks begin to interpenetrate each other, the regions that overlap first, e.g. region 6, may have more of the gravitationally unstable GMCs layers formed first, leading to in situ starburst first there. As the colliding/merging proceeds and the overlapping zone between the two colliding disks bulks up, cloud collisions from the two colliding disks spread to more and more regions, i.e. both the northwest (e.g. to regions 8, 9) and southeast (e.g. to regions 5, 4) of the *overlap* regions. This leads to progressively lagging starbursts triggered by the radiative shock compressions toward both the northwest and southeast directions of the *overlap* regions. In short, the identified sequential star formation paths could be the imprints of the interpenetrating process of the two colliding galaxy disks.

Both kinematic analysis (Hibbard et al. 2001) and numerical simulations (Toomre & Toomre 1972; Barnes 1988) suggest that the two galaxies of the Antennae system began their first close encounter several hundred million years ago, and the two colliding galaxies may have passed their

first close encounter (Mihos, Bothun & Richstone 1993). The first peak of large-scale starburst phase may have just passed in the Antennae (Mihos & Hernquist 1996), which can be evidenced by the moderate star formation strengths shown in Figs. 5 & 6, consistent with the star formation efficiency map across the whole system (Gao et al. 2001). While the moderate, continuous (recent) star formation for most regions is consistent with this scenario, the currently violent enhancement of star formation and the sequential star formation paths for the *overlap* regions may suggest that now the two colliding galaxies are just launching their second close encounter.

After analysing H₂ $\nu = 0 - 0$ S(3) $\lambda = 9.66 \mu\text{m}$ line emission obtained by ISOCAM CVF, Haas, Chini & Klaas (2005) found that both the southwestern and northwestern edges of the *overlap* regions, which are very close to the star-forming region 5 and regions 9, respectively, have exceptionally high $L(\text{H}_2)/L(\text{FIR})$ ratios that exceed that of all other known galaxies. But the absolute current/recent star formation there (especially the northwestern edge) are very weak, just as we find from population analysis (see Table 1 and 2). They suggest that the high H₂ emission there should be excited by pre-starburst shocks which are caused by cloud-cloud collisions. The low mass fractions of intermediate populations and the very high (age-averaged) mass ratios of young to intermediate populations for the two edges, especially the northwestern edge, indicate there indeed are very young star-forming sites, which are most probably to be triggered by pre-starburst shocks following the second close encounter between the two galaxies. However, recent high-quality observations from *Spitzer* (Brandl et al. 2009) detected about five times less integrated H₂ S(3) line flux than does ISOCAM CVF, and didn't find the previously claimed strong H₂ emission peak in the northern *overlap* zone. These new observations cast doubt on the pre-starburst shock origin of the H₂ emission in the *overlap* regions.

6 SUMMARY

To summarise, taking advantage of the availability of multiwavelength imagery from FUV to $24 \mu\text{m}$ from *GALEX*, *HST*, *2MASS* and *Spitzer* in both high resolution and high sensitivity:

- We compare the broadband SEDs of star-forming regions selected as $24 \mu\text{m}$ peaks across the whole merging disks of the Antennae galaxies, which provides us a basis to comprehend the complete picture of star formation histories. The large ratios of $24 \mu\text{m}/8 \mu\text{m}$ for the *overlap* regions and the blue, strong UV emission for the *western-loop* regions demonstrate that currently they are the most intense star-forming sites, although the *western-loop* regions are at a relatively later star formation stage compared to the *overlap* regions. Most of the other regions, which have redder *UB* color, weaker IR dust emission and UV emission, across the whole system are forming stars at a quite moderate level during the past ~ 100 Myr.

- We roughly constrain the star formation histories of these active star-forming regions across the whole system, with the degeneracy between stellar population and extinction broken, by including $24 \mu\text{m}$ dust emission into population analysis. Compared with other regions, the *over-*

lap regions are now experiencing much more violent enhancement of star formation, although both the *overlap* and the *western-loop* regions are the most intense *current* star-forming sites across the whole system. Our analysis is in general agreement with the findings of Gao et al. (2001), i.e. except for some localized violent starbursts confined mainly in the *overlap* regions and the *western-loop* regions of NGC 4038, the bulk of star formation is at a moderate level comparable to that of star-forming regions in quiescently star-forming galaxies.

- We suggest two sequential star formation paths across the famous *overlap* regions, which may reflect the (second) interpenetrating process of the second passage between the two colliding galaxy disks. We also suggest that the recent star formation of both the northern and southern edges of the *overlap* zone might be just triggered by pre-starburst shocks.

- We report the nonnegligible ($> 18\%$) excess emission contribution to the total IRAC $4.5 \mu\text{m}$ for the whole system. The well-known brightest MIR “hotspot” in the *overlap* regions has total $4.5 \mu\text{m}$ emission ($\geq 80\%$ excess emission) even higher (by $\sim 20\%$) than that of the nuclear region of NGC 4039 and nearly equals to that of the nuclear region of northern galaxy NGC 4038. The unusually low ratio of $3.6 \mu\text{m}/4.5 \mu\text{m}$ implies that, in addition to hot dust emission, other emission mechanisms, such as atomic fine-structure lines and vibrationally excited molecular hydrogen lines from dense PDRs, have significant contribution to IRAC $4.5 \mu\text{m}$.

ACKNOWLEDGEMENTS

We thank the anonymous referee who provided extremely useful comments that resulted in substantial improvements to the presentation of the paper. We are grateful to Y. H. Zhao and X. Z. Zheng for useful discussions and suggestions that helped improve the presentation of this paper. Research for this project is supported by NSF of China (Distinguished Young Scholars #10425313, grants #10833006 & #10621303), Chinese Academy of Sciences' Hundred Talent Program, and 973 project of the Ministry of Science and Technology of China (grant #2007CB815406). XK is supported by the National Natural Science Foundation of China (NSFC, Nos. 10633020, and 10873012), the Knowledge Innovation Program of the Chinese Academy of Sciences (No. KJCX2-YW-T05), and National Basic Research Program of China (973 Program; No. 2007CB815404). This research has made use of the NED which is operated by the JPL. Archival data from *GALEX*, *HST*, *2MASS* and *Spitzer* have also been used for the research.

REFERENCES

- Alonso-Herrero A., Rieke G. H., Rieke M. J., Colina L., Perez-Gonzalez P. G., Ryder S. D., 2006, *ApJ*, 650, 835
 Anders P., & Fritze-v. Alvensleben U., 2003, *A&A*, 401, 1063
 Barnes J. E., 1988, *ApJ*, 331, 699
 Bastian N., Emsellem E., Kissler-Patig M., Maraston C., 2006, *A&A*, 445, 471

- Bastian N., Tranco G., Konstantopoulos L. S., Miller B. W., 2009, preprint (astro-ph/09062210)
- Bell E. F., 2003, *ApJ*, 586, 794
- Brandl B. R., Sniijders L., den Brok M. et al., 2009, preprint (astro-ph/09051058)
- Calzetti D., Kinney A. L., Storchi-Bergmann T., 1994, *ApJ*, 429, 582
- Calzetti D., Armus L., Bohlin R. C., Kinney A. L., Koornneef J., Storchi-Bergmann T., 2000, *ApJ*, 533, 682
- Calzetti D., Kennicutt R. C., Bianchi L. et al., 2005, *ApJ*, 633, 871
- Calzetti D., Kennicutt R. C., Engelbracht C. W. et al., 2007, *ApJ*, 666, 870
- Cardelli J. A., Clayton G. C., Mathis J. S., 1989, *ApJ*, 345, 245
- Charlot S., Fall S. M., 2000, *ApJ*, 539, 718
- Condon J. J., 1992, *ARA&A*, 30, 575
- Conselice C. J., Bershadsky M. A., Dickinson M., Papovich C., 2003, *AJ*, 126, 1183
- Conselice C. J., Chapman S. C., Windhorst R. A., 2003, *ApJ*, 596, L5
- Conselice C. J., Yang C., Bluck A. F. L., 2009, *MNRAS*, 394, 1956
- de Ravel L., Le Fevre O., Tresse L. et al., 2008, *A&A*, 498, 379
- Draine B. T., Li A., 2007, *ApJ*, 657, 810
- Elbaz D. M., Cesarsky C. J., 2003, *Science*, 300, 270
- Fabbiano G., Zezas A., Murray S. S., 2001, *ApJ*, 554, 1035
- Fabbiano G., Krauss M., Zezas A., Rots A., Neff S., 2003, *ApJ*, 598, 272
- Fabbiano G., Baldi A., King A. R., Ponman T. J., Raymond J., Read A., Rots A., Schweizer F., Zezas A., 2004, *ApJ*, 605, 21
- Fall S. M., Chandar R., Whitmore B. C., 2005, *ApJ*, 631, 133
- Fazio G. G., Hora J. L., Allen L. E. et al., 2004, *ApJS*, 154, 10
- Gao Y., Lo K. Y., Lee S. -W., Lee T. -H., 2001, *ApJ*, 548, 172
- Gao Y., Zhu M., Seaquist E. R., 2003, *AJ*, 126, 2171
- Gavazzi G., Bonfanti C., Sanvito G., Boselli A., Scodreggio M., 2002, *ApJ*, 576, 135
- Goodwin S. P., Bastian N., 2006, *MNRAS*, 373, 752
- Gordon K. D., Engelbracht C. W., Rieke G. H., Misselt K. A., Smith J. -D. T., Kennicutt R. C. Jr., 2008, *ApJ*, 682, 336
- Gilbert A. M., Graham J. R., McLean I. S. et al., 2000, *ApJ*, 533, 57
- Gilbert A. M., Graham J. R., 2007, *ApJ*, 668, 168
- Gil de Paz A., Boissier S., Madore B. F. et al., 2007, *ApJS*, 173, 185
- Haas M., Chini R., Klaas U., 2005, *A&A*, 17, L20
- Hibbard J. E., van der Hulst J. M., Barnes J. E., Rich R. M., 2001, *AJ*, 122, 2969
- Hibbard J. E., Bianchi L., Thilker D. A. et al., 2005, *ApJ*, 619, L87
- Holtzman J. et al., 1995, *PASP*, 107, 1065
- Hummel E., van der Hulst J. H., 1986, *A&A*, 155, 151
- Hughes A., Wong T., Ekers R., Staveley-Smith L., Filipovic M., Maddison S., Fukui Y., Mizuno N., 2006, *MNRAS*, 370, 363
- Jog C. J., Solomon P. M., 1992, *ApJ*, 387, 152
- Kartaltepe J. S., Sanders D. B., Scoville N. Z. et al., 2007, *ApJS*, 172, 320
- Knapen J. H., 1998, *MNRAS*, 297, 255
- Kennicutt R. C., Jr., Calzetti D., Walter F. et al., 2007, *ApJ*, 671, 333
- Kong X., Zhou X., Chen J. S. et al., 2000, *AJ*, 119, 2745
- Kong X., Charlot S., Brinchmann J., Fall S. M., 2004, *MNRAS*, 349, 769
- Kinney A. L., Bohlin R. C., Calzetti D., Panagia N., Wyse R. F. G., 1993, *ApJS*, 86, 5
- Kroupa P., 2002, in *ASPConf. Ser.285, Modes of Star Formation and the Origin of Field Populations*, ed.E.K.Grebel & W.Brandner (San Francisco: ASP), 86
- Kunze D., Rigopoulou D., Lutz D. et al., 1996, *A&A*, 315, L101
- Le Fevre O., Abraham R., Lilly S. J. et al., 2000, *MNRAS*, 311, 565
- Lin L., Patton D. R., Koo D. C. et al., 2008, *ApJ*, 681, 232
- Lu N. Y., Helou G., Tuffs R., Xu C., Malhotra S., Werner M. W., Thronson H., 1996, *A&A*, 315, L153
- Martin-Hernandez N. L., Peeters E., Damour F. et al., 2000, *ESASP*, 456, 135
- Mirabel L. F., Vigroux L., Charmandaris V. et al., 1998, *A&A*, 333, L1
- Mengel S., Lehnert M. D., Thatte N., Tacconi-Garman L. E., Genzel R. 2001, *ApJ*, 550, 280
- Mengel S., Lehnert M. D., Thatte N., Tacconi-Garman L. E., Genzel R., 2002, *ApJ*, 383, 137
- Mengel S., Lehnert M. D., Thatte N., Genzel, R., 2005, *A&A*, 443, 41
- Mihos J. C., Bothun G. D., Richstone D. O., 1993, *ApJ*, 418, 82
- Mihos J. C., Hernquist L., 1996, *ApJ*, 464, 641
- Murphy E. J., Braun R., Helou G. et al., 2006, *ApJ*, 638, 157
- Nikola T., Genzel R., Herrmann F., Madden S. C., Poglitsch A., Geis N., Townes C. H., Stacey G. J., 1998, *ApJ*, 504, 749
- Neff S. G., Ulvestad J. S., 2000, *AJ*, 120, 670
- Oey M. S., Parker J. S., Mikles V. J., Zhang X. L., 2003, *AJ*, 126, 2317
- Peeters E., Martin-Hernandez N. L., Damour F. et al., 2002, *A&A*, 381, 571
- Patton D. R., Pritchett C. J., Carlberg R. G. et al., 2002, *ApJ*, 565, 208
- Read A. M., Ponman T. J., Wolstencraft R. D., 1995, *MNRAS*, 277, 397
- Rieke G. H., Young E. T., Engelbracht C. W. et al., 2004, *ApJS*, 154, 25
- Sanders D. B., Mirabel I. F., 1996, *ARA&A*, 34, 749
- Sanders D. B., Mazzarella J. M., Kim D. -C., Surace J. A., Soifer B. T., 2003, *ApJ*, 126, 1607
- Saviane I., Momany Y., da Costa G. S., Rich R. M., Hibbard J. E. 2008, *ApJ*, 678, 179
- Schweizer F., Burns C. R., Madore B. F., et al., 2008, *AJ*, 136, 1482
- Schlegel D. J., Finkbeiner D. P., Davis M., 1998, *ApJ*, 500, 525
- Schulz A., Henkel C., Muders D., Mao R. Q., Rollig M., Mauersberger R., 2007, *A&A*, 466, 467
- Smith J. D. T., Draine B. T., Dale D. A. et al., 2007, *ApJ*, 656, 770

- Stetson P. B. 1987, PASP, 99, 191
Thilker D. A., Boissier S., Bianchi L. et al., 2007, ApJ, 173, 572
Toomre A., Toomre J., 1972, ApJ, 178, 623
Vazquez G. A., Leitherer C., 2005, ApJ, 621, 695
Vigroux L., Mirabel F., Altieri B. et al., 1996, A&A, 315, L93
Wang Z., Fazio G. G., Ashby M. L. N. et al., 2004, ApJS, 154, 193
Wilson C. D., Scoville N., Madden S. C., Charmandaris V. 2000, ApJ, 542, 120
Wilson C. D., Scoville N., Madden S. C., Charmandaris V. 2003, ApJ, 599, 1049
Whitmore B., Schweizer F., 1995, AJ, 109, 960
Whitmore B. C., Zhang Q., Leitherer C., Fall S. M., Schweizer F., Miller B. W., 1999, AJ, 118, 1551
Whitmore B. C., Zhang Q., 2002, AJ, 124, 1418
Whitmore B. C., 2004, in *The Formation and Evolution of Massive Young Star Clusters*, ASPC, 322, 419
Yun M. S., Reddy N. A., Condon J. J., 2001, ApJ, 554, 803
Zhang Q., Fall M., Whitmore B. C., 2001, ApJ, 561, 727
Zhu M., Gao Y., Seaquist E. R., 2007, AJ, 134, 118